

Tails of Instability and Decay: a Hydrodynamic Perspective

Olalla A. Castro-Alvaredo,¹ Cecilia De Fazio,¹ Benjamin Doyon,² and Aleksandra A. Ziolkowska³

¹*Department of Mathematics, City, University of London,
10 Northampton Square, EC1V 0HB London, UK*

²*Department of Mathematics, King's College London, Strand WC2R 2LS, UK*

³*Rudolf Peierls Centre for Theoretical Physics, University of Oxford, Parks Road, Oxford OX1 3PU, UK*

(Dated: December 23, 2024)

In the context of quantum field theory (QFT), unstable particles are associated with complex-valued poles of two-body scattering matrices in the unphysical sheet of rapidity space. The Breit-Wigner formula relates this pole to the mass and life-time of the particle, observed in scattering events. In this letter, we uncover new, dynamical signatures of unstable excitations and show that they have a strong effect on the non-equilibrium properties of QFT. Focusing on a 1+1D integrable model, and using the theory of Generalized Hydrodynamics, we study the formation and decay of unstable particles by analysing the release of hot matter into a low-temperature environment. We observe the formation of tails and the decay of the emitted nonlinear waves, in sharp contrast to the situation without unstable excitations. We expect these signatures of instability to have a large degree of universality. Our study shows that the out-of-equilibrium dynamics of many-body systems can be strongly affected not only by the spectrum, but also by excitations with finite life-times.

Introduction.— Physics far from equilibrium has received a large amount of interest recently. It is now understood that non-equilibrium dynamics offers a powerful new way of studying strongly correlated many-body systems, as it brings out properties that can be hidden in equilibrium situations. This viewpoint has gained strong traction, particularly in one dimension [1–8]. It is interesting to apply this principle to quantum field theory (QFT) far from equilibrium. A paradigm is that the essence of quantum dynamics in QFT is accessed by scattering theory, describing how few particles interact [9–11]. But scattering events – perhaps the simplest example of non-equilibrium dynamics – mainly teach us about the vacuum state, and what happens at low densities. Further, in the context of applications to many-body systems, scattering experiments are difficult to implement. Dynamics with finite energy and spatial particle densities can be argued to be more common and accessible, and to have a richer physics.

A case in point is the spectrum of asymptotic particles. This is a basic ingredient of scattering theory, but it is not sufficient in order to fully understand finite-density physics. Other emergent structures of QFT may play an important role. One example is the phenomenon of confinement, which taps into the internal structure of asymptotic particles. As found in [12–14] this and other qualitatively similar [15] phenomena can be linked quite explicitly to the non-equilibrium dynamics that follows so-called quantum quenches [16, 17]. Another phenomenon, only indirectly observed in scattering events, is the existence of particles with finite life-times, which are absent from the asymptotic spectrum. Technically, they appear as poles in the unphysical sheet of the analytically continued scattering phase function [11]. The Breit-Wigner formula allows one to evaluate their mass and life-time from the position of this pole [18]. At nonzero tempera-

tures, physical intuition suggests that unstable particles are constantly formed and destroyed, and thus truly exist in finite proportions. As such, they may be expected to have a strong effect on the dynamics far from equilibrium at finite densities.

In this letter, we argue that this is the case, by studying the propagation of nonlinear waves at finite energy densities. We focus on a 1+1D integrable QFT, which admits one unstable particle interpreted as a loosely bound state of two different asymptotic particle types. Partly mimicking the vacuum scattering physics, we analyse the setup where a high-temperature finite region, with enough energy to form a large number of unstable particles, is released into a colder environment, with few unstable particles. We study the emitted waves and their large-time behaviour by numerically solving the associated hydrodynamic equations. At the energies considered, asymptotic particles have velocities extremely near to the speed of light (set to $c = 1$). Then, the standard picture, without unstable particles, is that after the splitting of the initial high-temperature region, long-lived, well-localised regions of higher energy density propagate at unit velocity in both directions (if the colder environment is the vacuum, over extremely long times, the waves would slowly decompose into their asymptotic particle content). We argue that the formation, propagation and decay of unstable particles drastically modifies this dynamics. Three main observations are made: (a) the emitted waves *partially decay* after the splitting of the initial high-temperature region, representing the rapid decay of unstable particles; (b) long tails appear, trailing the well localised high-density waves; and (c) in an environment with nonzero temperature, new persistent waves emerge, interpreted as being residual *stable* populations of unstable particles.

Our analysis demonstrates that non-equilibrium setups

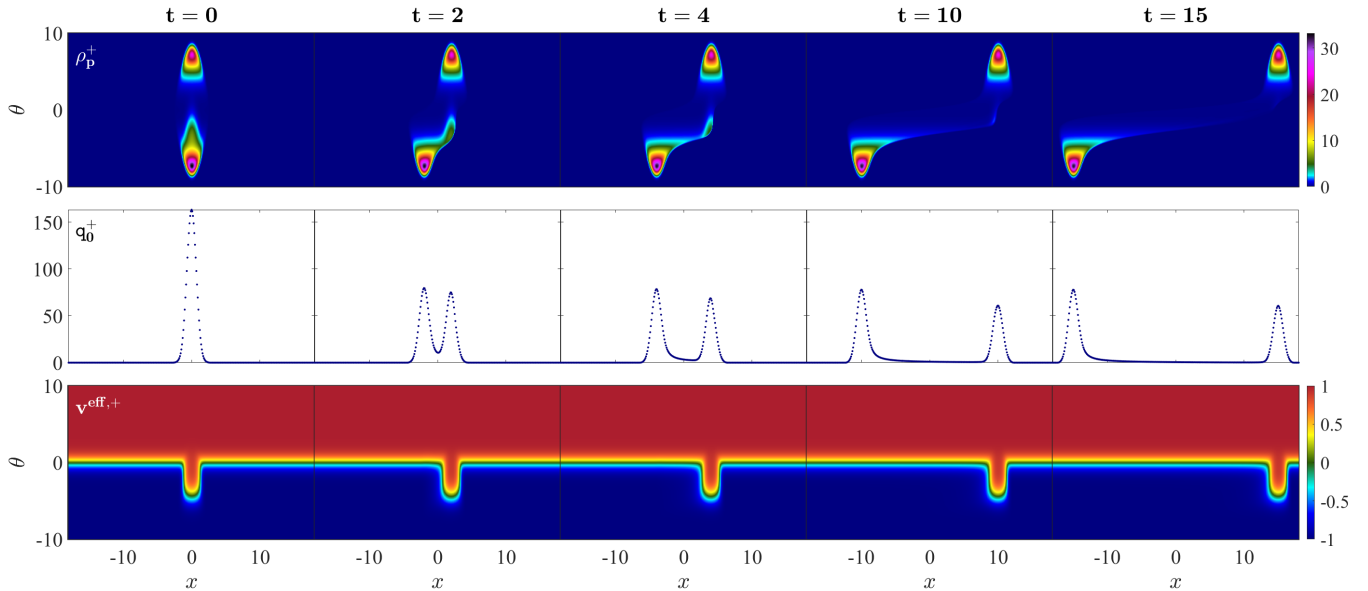


FIG. 1. Particle + dynamics for various time snapshots. The parameters are $\sigma = 10$, $T_a = 0$ (no bath) and $2T_m = e^7$. Row 1: Spectral density exhibiting three characteristic local maxima, the least of which decays in time leading to the formation of a tail. Row 2: Spatial particle density exhibiting both a tail and decay. Row 3: Effective velocities dominated by the values ± 1 but exhibiting an intermediate plateau in rapidity space which is correlated with the decaying peak of the spectral density. The dynamics of particle $-$ follows from the relations: $\rho_p^+(x, t, \theta) = \rho_p^-(-x, t, -\theta)$, $q_0^+(x, t) = q_0^-(-x, t)$ and $v^{\text{eff},+}(x, t, \theta) = -v^{\text{eff},-}(-x, t, -\theta)$.

at finite energy densities allow a more direct observation of unstable particles. It also shows that their presence leads to new asymptotically stable waves, suggesting that they may play the role of stable excitations in an effective scattering theory at finite densities.

Model and Hydrodynamic Equations.— Many new applications of 1+1D quantum integrable models have emerged over the past two decades. Originally regarded as toy models with rich underlying mathematical structures, they now play a role in many areas of modern theoretical physics: from the emergence of integrability in the context of string/gauge theories [19], to the experimental realisation of quantum integrable structures [20, 21], to the resulting measurement of quantities that can be directly compared to analytic formulae [22, 23]. The investigation of the out-of-equilibrium dynamical features of quantum integrable models, largely spurred by the Quantum Newton’s Cradle experiment [24], has become an active area of research [25]. In particular, generalised hydrodynamics (GHD) [26, 27], the hydrodynamic theory which accounts for the extensive amount of conserved charges and generalized thermalisation (GGE) [28] in quantum integrable models, have been very successful (see e.g. [8] for a recent review).

Integrability implies that multi-particle scattering is elastic and factorises into two-body events [29–31]. Interestingly, these constraints do not forbid the existence of unstable bound states even if few theories with this feature are known. In this letter, we use the GHD ap-

proach to study a model whose two-body S -matrix has a pole in the rapidity’s unphysical sheet, which, as mentioned, implies the presence of an unstable particle. In a previous work [32] it was found that the presence of this unstable excitation gives distinctive features of various hydrodynamic quantities both at equilibrium and in non-equilibrium steady states. In the current work we demonstrate that the formation and decay of unstable excitations can be dynamically observed within the GHD framework.

The model under study is known as the $SU(3)_2$ -homogenous sine-Gordon (HSG) model and has a spectrum of two self-conjugate particles. One particularity is that its S -matrix breaks parity invariance. It constitutes the simplest of a large family of theories, the G_k -HSG models labelled by a simply-laced algebra G and an integer index k called the level. The integrability and S -matrix of these theories were studied in a series of works [33–36]. Thereafter, much work was devoted to the computation of form factors [37–40], the application of the thermodynamic Bethe ansatz [41–43], and the study of mass-coupling relations [44, 45].

The GHD equations depend on specific features of the model through the two-body scattering phases:

$$\varphi_{\pm\pm}(\theta) = 0, \quad \varphi_{\pm\mp}(\theta) = \text{sech}(\theta \pm \sigma), \quad \sigma \in \mathbb{R} \quad (1)$$

where θ is the rapidity difference among particles and \pm label the particle species. Particles \pm have equal mass m . The Breit-Wigner formula predicts the formation of an

unstable particle with mass and decay width both proportional to $e^{|\sigma|/2}$ for $|\sigma| \gg 0$. For σ positive the scattering phases dictate that a particle \pm has maximum interaction with a particle \mp if it hits it from the right/left and their rapidity difference is of order $\theta = \mp\sigma$. This feature means that interaction for each particle is maximised for either positive or negative rapidities, whereas particles behave as free fermions otherwise. In addition, each particle species interacts with its own kind always as a free fermion. Thus, in a Gibbs ensemble at temperature $1 \ll T \ll e^{|\sigma|/2}$ the theory flows to a conformal field theory of central charge $c = 1$ corresponding to two free fermions whereas for $T \gg e^{|\sigma|/2}$ it flows to an interacting theory with central charge $c = 6/5$ [33]. The larger number of degrees of freedom at high temperatures is linked to the presence of a finite proportion of unstable particles in the thermal state, allowed by the large energy.

The initial state is defined by a Gaussian temperature profile

$$T(x) = T_a + (T_m - T_a)e^{-x^2} \quad \text{with} \quad T_a, T_m \in \mathbb{R}_{\geq 0}, \quad (2)$$

where x is the space coordinate. From now on, we will refer to T_a as the bath temperature. Given such an initial configuration, the dynamics can be obtained by GHD as described for instance in [46–49]. In GHD, asymptotic particles, characterised by their rapidity θ and quantum number b , are “dressed”, within finite density states, into fluid modes. The state at any space-time point x, t is then described by an occupation function $n^b(x, t, \theta)$. The thermodynamic Bethe ansatz [52] allows us to evaluate the initial condition $n^b(x, 0, \theta)$ from (2) using the local density approximation. For our analysis, the three quantities of interest are the phase-space (or spectral) density of particles $\rho_p^\pm(x, t, \theta)$, the spatial particle density $q_0^\pm(x, t)$, and the effective velocity $v^{\text{eff}, b}(x, t, \theta)$, which is the fluid velocity of mode θ, b . They are defined as

$$\rho_p^\pm(x, t, \theta) = e^{\text{dr}, \pm}(x, t, \theta)n^\pm(x, t, \theta), \quad (3)$$

$$q_0^\pm(x, t) = \int_{-\infty}^{\infty} \frac{d\theta}{2\pi} \rho_p^\pm(x, t, \theta), \quad (4)$$

$$v^{\text{eff}, \pm}(x, t, \theta) = p^{\text{dr}, \pm}(x, t, \theta)/e^{\text{dr}, \pm}(x, t, \theta). \quad (5)$$

Here $e^\pm(\theta) = \cosh \theta$ is the energy, and $p^\pm(\theta) = \sinh \theta$ the momentum (the mass is set to unity). The dressing operation “dr” is defined by the equations

$$\sum_{b=\pm} \int_{-\infty}^{\infty} \frac{d\alpha}{2\pi} G_b^\pm(\theta, \alpha) h^{\text{dr}, b}(x, t, \alpha) = h^\pm(\theta), \quad (6)$$

with

$$G_b^\pm(\theta_2, \theta_1) = 2\pi \delta(\theta_{12}) \delta_{b\pm} - \varphi_{\pm\mp}(\theta_{12}) n^b(x, t, \theta_1) \delta_{b\mp}, \quad (7)$$

and $\theta_{12} := \theta_1 - \theta_2$. The occupation functions evolve according to the GHD equation [26, 27]

$$\partial_t n^\pm(x, t, \theta) + v^{\text{eff}, \pm}(x, t, \theta) \partial_x n^\pm(x, t, \theta) = 0. \quad (8)$$

In free theories $v^{\text{eff}}(x, t, \theta) = \tanh \theta$, and therefore, at large temperatures, where large rapidities are involved, excitations mostly move at velocities ± 1 . Typically, interaction of the kind we find in most integrable QFTs, does not qualitatively change the effective velocity, and the same holds near interacting conformal points. This leads to the splitting of the original density maximum at $x = 0$ into two identical maxima propagating in opposite directions [46–49]. This is in fact also the phenomenology of non-integrable models, where the dynamics is dominated by two “sound modes”. We will see that the presence of unstable particles modifies this picture substantially.

Numerical Results.— In order to obtain numerical results, we adapted the iFluid package [53], a MATLAB code that solves GHD for a wide range of conditions and models. More details are presented in the supplementary material. We have chosen $\sigma = 10$, which means that for temperatures $2T \lesssim e^5$ the model describes two free Majorana fermions, while at higher temperatures unstable particles are formed. In order to best observe this threshold, we have chosen a bath temperature T_a which is either 0 or within the free fermion regime $2T_a = e^3$, and a maximum temperature $2T_m = e^7$ which is within the interacting region. As emphasised in [32], the analysis of spectral densities is helpful in determining the composition of finite-density states.

Let us start by considering results in a zero-temperature environment in FIG. 1. The first row illustrates the behaviour of the spectral density of particle $+$ as a function of time. At time $t = 0$ we observe many of the equilibrium features we would encounter for a Gibbs ensemble at the highest temperature T_m . These were first discussed in [32]: there are three local maxima centred around rapidities $\theta \approx \pm \log(2T_m) = \pm 7$ and $\theta \approx \log(2T_m) - \sigma = -3$. Due to the structure of the scattering phases (1), the maximum at $\theta \approx 7$ is the free fermion solution (free fermion peak), the maximum at $\theta \approx -7$ (interacting peak) is higher, and its additional size compared to the free fermion peak is a signature of the presence of interaction, and the maximum at $\theta \approx -3$ (subsidiary peak) is a consequence of interaction with the interacting peak of particle $-$; it would not be present for free fermions. The subsidiary peak represents the proportion of particles $+$ loosely involved in a bind with particles $-$: these are the unstable particles. As we can see from the effective velocity figure in the third row, for $t = 0$ the interacting peak moves at speed -1 , the free fermion peak moves at speed $+1$ and the subsidiary peak contains less particles, and a spectrum of positive and negative effective velocities (captured by the “rainbow” colouring and the presence of an intermediate plateau of the effective velocity centred at $\theta = -\sigma/4 = -2.5$). The subsidiary peak contains a proportion of particles with velocities near to $+1$, which is the speed of the particle $-$ interacting peak, further suggesting the presence of a

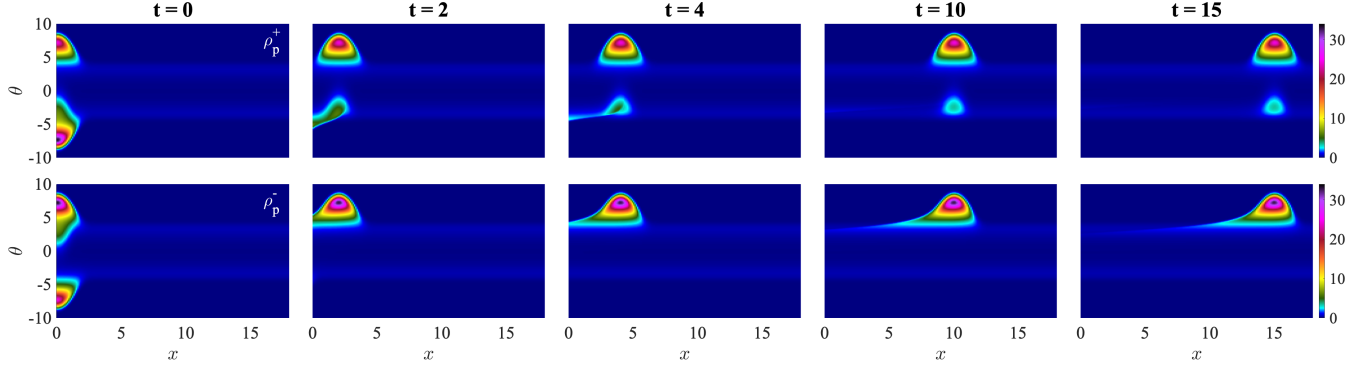


FIG. 2. Snapshots of the spectral densities $\rho_p^\pm(x, t, \theta)$ for $x \geq 0$ in the presence of a bath at temperature $2T_a = e^3$, $\sigma = 10$ and $2T_m = e^7$. Recall that $\rho_p^+(x, t, \theta) = \rho_p^-(x, t, -\theta)$. Whilst the interacting and free fermion peaks remain largely unchanged, the bath facilitates the formation of a persistent peak that travels at speed +1 “riding” on the bath. The two light-blue ridges are also due to the bath whose temperature is in the free fermion region of the theory. The ridges look “static” because they are uniformly distributed in space but represent particles propagating with opposite effective velocities ± 1 . See also the videos [50, 51].

population of unstable particles (this group has velocities near to +1).

Turning on time, the salient feature is that the subsidiary peak moves as per the initial splitting, but then falls apart, leaving behind a tail of slow particles. Unstable particles start moving at speed near +1, but, as they enter the zero-temperature environment, decay faster than they can form, and we see the particle + components un-binding and recovering their non-interacting speeds near to -1 . Note that the initial spread of effective velocities in the subsidiary peak, and the consequent dispersion, is not enough in order to explain its falling apart: the zero-temperature surrounding bath, with a very different effective velocity profile, leads to the decay of unstable particles, which is the dominant effect.

As shown in the second row of FIG. 1, features of the spatial particle density reflects this physics. After the initial splitting, the right-moving wave reduces in time, leaving just the free fermion contribution (which remains unchanged for larger times) and a tail attached to the left-moving wave at $x < 0$. This is accentuated by concentrating on negative rapidities, see the inset of FIG. 3. The formation of tails and decay of local maxima in spatial densities are features that identify the presence of unstable particles.

We next investigate whether any of these behaviours change substantially in the presence of a bath at nonzero temperature. FIG. 2 shows the $x \geq 0$ part of the functions $\rho_p^\pm(x, t, \theta)$ (see also the video [50]). Two main changes occur. First, two continuous, static ridges are formed centred around $\theta \approx \pm \log(2T_a) = \pm 3$: the free fermion equilibrium distribution for temperature T_a . Second, the subsidiary peak observed at time $t = 0$ no longer fully disintegrates under time evolution. Instead, it largely persists, propagating on top of the $\theta = -3$ ridge. The presence of this persisting peak has a very in-

teresting physical interpretation. Because of the spread of velocities in the initial subsidiary peak, it cannot be explained by a large population of particles at constant velocity +1. Why is this wave travelling at speed +1, riding on the bath? The answer is that the large wave of particles – going at velocity +1 interacts with particles + in the bath, something that is possible because they are present around the rapidities of the subsidiary peak. They form unstable particles as they pass by, thus changing the bath density. The resulting effect is akin to having a fluid that is magnetic, and running a magnet pass it. We see a wave that follows the magnet but the fluid itself does not need to move. This is a hydrodynamic effect never previously seen in the GHD context. It is also worth pointing out that the life-time of the unstable particles is of order $e^{-\frac{\sigma}{2}}$ and that the persisting peak represents a constant density of unstable particles, that is, particles rapidly decay and reform within this density, with the end result of preserving it for large times.

The effect of the bath is seen starkly in FIG. 3 (see also the video [51]). Here we plot the “partial” spatial particle density for particle + resulting from integrating the spectral density for $\theta < 0$. Leaving out $\theta > 0$ is equivalent to subtracting the contribution of the free fermion peak which remains unchanged for all times. FIG. 3 renders both the decay of the subsidiary peak in the absence of a bath (inset) and its persistence in the presence of a bath (main figure) evident.

Discussion and Conclusion.— In this letter we have shown how unstable particles in integrable QFT can be seen in a new light within the GHD framework. The presence of an unstable excitation substantially alters the features of the densities and effective velocities associated to its stable constituents; notably, a new local maximum of the spectral density emerges. An analysis of this local maximum and its disintegration shows that, after release

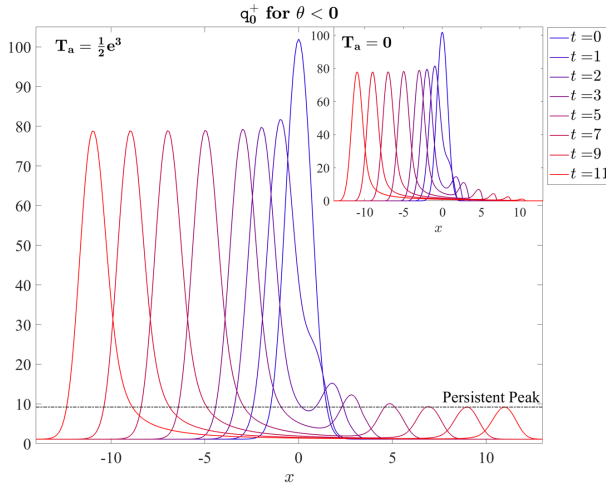


FIG. 3. The “partial” spatial particle density $q_0^+(x, t)$ obtained from integrating $\rho_p^+(x, t, \theta)$ for $\theta < 0$ showing the decay (no bath, inset) and persistence (bath, main figure) of the subsidiary peak. See also the video [51].

into a zero- or low-temperature environment, unstable particles decay. In spatial density profiles, this is hallmark by the slow decay of propagating waves and the formation of tails. Importantly, in the presence of a bath, a new hydrodynamic phenomenon comes into play. We find the long-time persistence of a small but significant wave of unstable particles “riding” on top of the bath, propelled by its interaction with the large wave of particles of the opposite type.

We have chosen temperatures that are large enough so that the presence of a continuum of fluid modes in integrable systems does not play an important role. The physics is dominated by the flow between a free ($c = 1$) and interacting ($c = 6/5$) conformal field theory, representing the formation and decay of unstable particles. The distinct signatures of instability identified within GHD are explained via the combined phenomenology of unstable particles and hydrodynamics, and should reflect universal behaviours.

Given how rich the dynamics of this simple model is, it would be very interesting to study other models where more unstable particles with tunable masses and decay widths are present. There is also still much to learn about the time evolution of hydrodynamic quantities under variation of T_a, T_m and σ , which we hope to address in [54]. The present work paves the way for identifying signatures of unstable particles experimentally.

Acknowledgements.— We are grateful to Frederik S. Møller for answering our questions on the iFluid package. In 2020 two groups of courageous colleagues put together the conference “Great Lessons from Exact Techniques and Beyond” held in Padova 20–25 September 2020 and the summer school on “Clean and disordered systems out of equilibrium” held in Cargèse 14–18 September 2020.

We thank the organisers of both, for their financial support, for giving us the opportunity to meet in person and discuss and, especially, for creating islands of normality in the midst of a global pandemic.

- [1] J. Eisert, M. Friesdorf, and C. Gogolin, Quantum many-body systems out of equilibrium, *Nature Phys.* **11**(2), 124–130 (2015).
- [2] F. H. L. Essler and M. Fagotti, Quench dynamics and relaxation in isolated integrable quantum spin chains, *J. Stat. Mech.* **2016**(6), 064002 (2016).
- [3] R. Vasseur and J. E. Moore, Nonequilibrium quantum dynamics and transport: from integrability to many-body localization, *J. Stat. Mech.* **2016**(6), 064010 (2016).
- [4] E. Ilievski, M. Medenjak, T. Prosen, and L. Zadnik, Quasilocal charges in integrable lattice systems, *J. Stat. Mech.* **2016**(6), 064008 (2016).
- [5] D. Bernard and B. Doyon, Conformal field theory out of equilibrium: a review, *J. Stat. Mech.* **2016**(6), 064005 (2016).
- [6] L. D’Alessio, Y. Kafri, A. Polkovnikov, and M. Rigol, From quantum chaos and eigenstate thermalization to statistical mechanics and thermodynamics, *Adv. in Phys.* **65**(3), 239–362 (2016).
- [7] C. Gogolin and J. Eisert, Equilibration, thermalisation, and the emergence of statistical mechanics in closed quantum systems, *Reports on Progress in Physics* **79**(5), 056001 (2016).
- [8] B. Doyon, Lecture notes on Generalised Hydrodynamics, *SciPost Phys. Lecture Notes* (2020).
- [9] M. Peskin and D. Schröder, An Introduction To Quantum Field Theory, *Frontiers in Physics* (1995).
- [10] S. Weinberg, The Quantum Theory of Fields, Cambridge University Press, Cambridge (1995).
- [11] R. Eden, P. Landshoff, D. Olive, and J. Polkinghorne, The Analytic S-Matrix, Cambridge University Press (1998).
- [12] M. Kormos, M. Collura, G. Takács, and P. Calabrese, Real-time confinement following a quantum quench to a non-integrable model, *Nature Phys.* **13**, 246–249 (2017).
- [13] N. J. Robinson, A. J. A. James, and R. M. Konik, Signatures of rare states and thermalization in a theory with confinement, *Phys. Rev. B* **99**(19) (2019).
- [14] Z.-C. Yang, F. Liu, A. V. Gorshkov, and T. Iadecola, Hilbert-Space Fragmentation from Strict Confinement, *Phys. Rev. Lett.* **124**, 207602 (2020).
- [15] O. A. Castro-Alvaredo, M. Lencsés, I. M. Szécsényi, and J. Viti, Entanglement Oscillations near a Quantum Critical Point, *Phys. Rev. Lett.* **124**(23) (2020).
- [16] P. Calabrese and J. L. Cardy, Evolution of entanglement entropy in one-dimensional systems, *J. Stat. Mech.* **0504**, P04010 (2005).
- [17] P. Calabrese and J. L. Cardy, Time-dependence of correlation functions following a quantum quench, *Phys. Rev. Lett.* **96**, 136801 (2006).
- [18] G. Breit and E. Wigner, Capture of Slow Neutrons, *Phys. Rev.* **49**(7), 519–531 (1936).
- [19] N. Beisert, C. Ahn, L. F. Alday, Z. Bajnok, J. M. Drummond, L. Freyhult, N. Gromov, R. A. Janik, V. Kazakov, T. Klose, and et al., Review of AdS/CFT Integrability:

An Overview, *Lett. in Math. Phys.* **99**(1-3), 3–32 (2011).

[20] M. T. Batchelor and A. Foerster, Yang–Baxter integrable models in experiments: from condensed matter to ultracold atoms, *J. Phys. A* **49**(17), 173001 (2016).

[21] F. A. Vind, A. Foerster, I. S. Oliveira, R. Sarthour, D. Soares-Pinto, A. M. Souza, and I. Roditi, Experimental realization of the Yang-Baxter Equation via NMR interferometry, *Sci. Rep.* **6**(20789) (2016).

[22] Z. Wang, J. Wu, W. Yang, A. K. Bera, D. Kamenskyi, A. T. M. N. Islam, S. Xu, J. M. Law, B. Lake, C. Wu, and A. Loidl, Experimental observation of Bethe strings, *Nature* **554**(7691), 219–223 (2018).

[23] M. Schemmer, I. Bouhoule, B. Doyon, and J. Dubail, Generalized Hydrodynamics on an Atom Chip, *Phys. Rev. Lett.* **122**, 090601 (2019).

[24] T. Kinoshita, T. Wenger, and D. Weiss, A Quantum Newton’s Cradle, *Nature* **440**, 900 (2006).

[25] J. Eisert, M. Friesdorf, and C. Gogolin, Quantum many-body systems out of equilibrium, *Nature Phys.* **11**, 124 (2015).

[26] O. A. Castro-Alvaredo, B. Doyon, and T. Yoshimura, Emergent hydrodynamics in integrable quantum systems out of equilibrium, *Phys. Rev. X* **6**(4), 041065 (2016).

[27] B. Bertini, M. Collura, J. De Nardis, and M. Fagotti, Transport in Out-of-Equilibrium XXZ Chains: Exact Profiles of Charges and Currents, *Phys. Rev. Lett.* **117**(20), 207201 (2016).

[28] M. Rigol, V. Dunjko, V. Yurovsky, and M. Olshanii, Relaxation in a Completely Integrable Many-Body Quantum System: An Ab Initio Study of the Dynamics of the Highly Excited States of 1D Lattice Hard-Core Bosons, *Phys. Rev. Lett.* **98**, 050405 (2007).

[29] A. Zamolodchikov and A. Zamolodchikov, Factorized S-matrices in two-dimensions as the exact solutions of certain relativistic quantum field models, *Ann. Phys.* **120**, 253–291 (1979).

[30] P. Dorey, Exact S matrices, in *Eotvos Summer School in Physics: Conformal Field Theories and Integrable Models*, pages 85–125, 8 (1996).

[31] G. Mussardo, Statistical Field Theory: An Introduction to Exactly Solved Models in Statistical Physics, Oxford Graduate Texts (2009).

[32] O. A. Castro-Alvaredo, C. De Fazio, B. Doyon, and F. Ravanini, On the hydrodynamics of unstable excitations, *JHEP* **2020**(45) (2020).

[33] C. R. Fernandez-Pousa, M. V. Gallas, T. J. Hollowood, and J. L. Miramontes, Solitonic integrable perturbations of parafermionic theories, *Nucl. Phys.* **B499**, 673–689 (1997).

[34] C. R. Fernandez-Pousa, M. V. Gallas, T. J. Hollowood, and J. L. Miramontes, The symmetric space and homogeneous sine-Gordon theories, *Nucl. Phys.* **B484**, 609–630 (1997).

[35] C. R. Fernandez-Pousa and J. L. Miramontes, Semi-classical spectrum of the homogeneous sine-Gordon theories, *Nucl. Phys.* **B518**, 745–769 (1998).

[36] J. L. Miramontes and C. R. Fernandez-Pousa, Integrable quantum field theories with unstable particles, *Phys. Lett.* **B472**, 392–401 (2000).

[37] O. A. Castro-Alvaredo, A. Fring, and C. Korff, Form factors of the homogeneous sine-Gordon models, *Phys. Lett.* **B484**, 167–176 (2000).

[38] O. A. Castro-Alvaredo and A. Fring, Identifying the operator content, the homogeneous sine- Gordon models, *Nucl. Phys.* **B604**, 367–390 (2001).

[39] O. A. Castro-Alvaredo and A. Fring, Renormalization group flow with unstable particles, *Phys. Rev.* **D63**, 021701 (2001).

[40] O. A. Castro-Alvaredo and A. Fring, Decoupling the $SU(N)_2$ homogeneous sine-Gordon model, *Phys. Rev.* **D64**, 085007 (2001).

[41] O. A. Castro-Alvaredo, A. Fring, C. Korff, and J. L. Miramontes, Thermodynamic Bethe ansatz of the homogeneous sine-Gordon models, *Nucl. Phys.* **B575**, 535–560 (2000).

[42] O. A. Castro-Alvaredo, J. Dreissig, and A. Fring, Integrable scattering theories with unstable particles, *Eur. Phys. J.* **C35**, 393–411 (2004).

[43] P. Dorey and J. Miramontes, Mass scales and crossover phenomena in the homogeneous sine-Gordon models, *Nucl. Phys.* **B697**, 405–461 (2004).

[44] Z. Bajnok, J. Balog, K. Ito, Y. Satoh, and G. Z. Tóth, On the mass-coupling relation of multi-scale quantum integrable models, *JHEP* **2016**(6) (2016).

[45] Z. Bajnok, J. Balog, K. Ito, Y. Satoh, and G. Z. Tóth, Exact Mass-Coupling Relation for the Homogeneous Sine-Gordon Model, *Phys. Rev. Lett.* **116**(18) (2016).

[46] V.B. Bulchandani, R. Vasseur, C. Karrasch, J.E. Moore, Solvable Hydrodynamics of Quantum Integrable Systems, *Phys. Rev. Lett.* **119**, 220604 (2017).

[47] B. Doyon, J. Dubail, R. Konik, and T. Yoshimura, Large-Scale Description of Interacting One-Dimensional Bose Gases: Generalized Hydrodynamics Supersedes Conventional Hydrodynamics, *Phys. Rev. Lett.* **119**(19) (2017).

[48] B. Doyon, H. Spohn, and T. Yoshimura, A geometric viewpoint on generalized hydrodynamics, *Nucl. Phys. B* **926**, 570–583 (2018).

[49] F. S. Møller, G. Perfetto, B. Doyon, and J Schmiedmayer, Euler-scale dynamical correlations in integrable systems with fluid motion, *SciPost Phys. Core* **3**, 016 (2020).

[50] Video: Time Evolution of Spectral Density versus the Effective Velocity in the Presence of a Bath, <https://youtu.be/mvNnzBL7vYs> .

[51] Video: Time Evolution of the Spectral Density with and without a Bath, <https://youtu.be/yyLcuTn4lBY> .

[52] A. Zamolodchikov, Thermodynamic Bethe ansatz in relativistic models. Scaling three state Potts and Lee-Yang models, *Nucl. Phys.* **B342**, 695–720 (1990).

[53] F. S. Møller and J. Schmiedmayer, Introducing iFluid: a numerical framework for solving hydrodynamical equations in integrable models, *SciPost Phys.* **8**(3) (2020).

[54] O. A. Castro-Alvaredo, C. De Fazio, B. Doyon, and A. A. Ziolkowska, Generalized Hydrodynamics of Unstable Excitations: Creation and Decay, In preparation (2021).

SUPPLEMENTARY MATERIAL

In this supplementary material we describe in more detail the numerical simulations presented in the paper, focussing on possible error sources, precision issues and consistency checks.

1 Generalities

As mentioned in the paper, our results have been obtained with iFluid (integrable-Fluid, version 1.1.0) which is an open-source MATLAB framework specifically designed for solving the GHD equations in integrable models [1]. It is worth mentioning also that an integral-equation solution to the GHD equation (8) (in the paper) is also known [2], but its numerical stability has not been sufficiently studied yet.

Thanks to a tensor-based numerical environment, iFluid boasts high efficiency and high process running speed. Additionally, a new model can be easily implemented by extending the iFluid package with a model-specific class. Such implementation can be done by following the instructions provided in [1]. However, the $SU(3)_2$ -HSG model requires additional modifications and we have implemented them in this study.

The quantities studied in this paper feature in the `iFluidCore` class, which provides solutions to the TBA equations and inputs for the GHD equations. By default, the definition of spatial particle density included in the `iFluidCore` class, depends on the type-array. It is a fundamental property of the class and is included in the model implementation as a one-dimensional array composed of integers which label the particle types. In massive integrable QFTs with more than one particle in the spectrum, this definition of the particle density introduces multiplicative factors in its type components, which can lead to wrong results. We have instead implemented the definition that reproduces the total spatial particle density $q_0(x, t) = q_0^+(x, t) + q_0^-(x, t)$ as defined in the main body of the paper and leads to a correct result. Moreover, in our implementation of the model, some `iFluidCore` functions have been modified to output the contributions from each particle type to a given quantity separately (i.e. the functions $q_0^\pm(x, t)$).

In iFluid, the propagation of the GHD quantities is computed via `iFluidSolver` class. In our numerical simulation we have employed the `SecondOrderSolver` solver, whose details can be found in section 3.2 in [1].

To the best of our knowledge, our work provides the first application of the iFluid package to a system which is initially prepared in a state involving temperatures $T \gg 1$. Earlier examples provided with the package (i.e. sinh-Gordon model) were tested for temperatures $T \approx 1$. We have successfully ensured the convergence of the thermodynamic Bethe ansatz equations evaluated by the `iFluidCore` class for temperatures up to $\mathcal{O}(e^{10})$. We have checked the consistency of our results in several ways.

2 Precision and Consistency Checks

In order to make sure that the modified code gave meaningful results we carried out various consistency checks, mainly comparing the outputs of iFluid with standard results that are accessible by other numerical procedures.

A preliminary check was done on the initial state, which is given by the solution of the (equilibrium) TBA equations for a given fixed temperature $T(x)$ for each value of x . In the iFluid code, the precision is controlled by two parameters, namely, the tolerance and the maximal number of iterations allowed. In order to guarantee the highest accuracy, we set the former to

10^{-32} and the latter to 5000. We made these choices in part by comparing the outputs of iFluid in the initial state to results obtained for the same functions with a Mathematica code used in [3], and established that, for the choices above, we achieved higher precision with iFluid.

A similar check was performed by evaluating the TBA scaling function $c(T)$ over a range of temperatures (especially at high temperatures), and seeing that plateaus at the expected values of the central charge [4] were reproduced. Likewise we computed the energy densities and currents in the UV (high temperature) limit, reproducing once more the results of [3].

t	0	3	6	9	12	15
Q_0	561.2520	561.2541	561.1937	561.1511	561.1156	561.0970

Table 1: Numerical values of the total particle density Q_0 at several times. Here, the parameters are: $\sigma = 10$, $\log(2T_m) = 7$ and $T_a = 0$ (no bath). To evaluate Q_0 , we have computed (4) in the main paper and performed a cubic spline interpolation, implementing additional grid points whose spacing in x is $\Delta x = 1. \times 10^{-5}$. Q_0 is numerically conserved, up to a variation on the first decimal place, which can be attributed to the discretisation procedure.

Having established that the ground state is accurately described, we then turned to consistency checks of dynamical quantities. We calculated the total particle density Q_0 given by the x -integral of the sum of partial densities in Eq.(4) of the main paper. Q_0 should be conserved in time and so its computation for various values of times provides a consistency check for numerical solutions of the GHD equations. In TABLE I we have reported the numerical values of the total particle density evaluated in the no-bath case. Q_0 is confirmed to be conserved, up to a numerical variation on the first decimal place, which is the order of the grid spacing implemented in the simulation (see TABLE II for details).

Finally, we performed other consistency checks which exploit the connection of our model with free theories. In particular, as explained in the main body of the paper, we have that for $T \ll e^{|\sigma|/2}$ our model should reduce to two Majorana free fermions. Thus, performing numerics for the $SU(3)_2$ -HSG model with $\sigma = 20$ for the same temperature choices discussed in this paper, we should obtain results which are fully in the free fermion regime where the GHD equations can be solved exactly. Thus, in this regime numerical results from iFluid can be compared to analytical solutions. We have confirmed that they are in perfect agreement.

3 Space and Rapidity Discretisations

Besides convergence of the numerical solution of the TBA equations, we have established that the key source of numerical error is the choice of space discretisation. The values adopted in our computations are given in Table 2.

We have devoted special attention to the discretisation of the rapidity interval. iFluid employs Gauss-Legendre quadrature integration, which has excellent convergence properties for integrals over a finite interval [5, 6]. However, this quadrature is optimised for minimising boundary errors. This means that the number of data intervals is lowest in the middle of the interval, precisely where we find the non-trivial behaviour of the thermodynamic quantities of interest. The dependence of the size of the rapidity intervals, $\Delta\theta$ on the rapidity θ and the number of points in the interval considered N for a fixed range of rapidities is shown in FIG. 4.

As a point of reference, we have chosen to compare the resolution at $\theta = 0$ and 10 , as a primary region with non-trivial dynamics. Although the discretisation interval for $\theta = 0$

	Δ_{\max}	No. Points	Max. Val.	Quadrature
t	0.2500	61	15.	Rectangular
x	0.1000	441	22.	Rectangular
θ	0.0762	700	17.	Gauss-Legendre

Table 2: Discretisation parameters and quadratures chosen for the two numerical simulations discussed in this paper (i.e. with and without a bath). From the left, the columns indicate (respectively for t, x, θ): the variable, the lowest resolution (i.e. the largest spacing between two grid points Δ_{\max}), the number of grid points, the largest absolute value the variable takes, and the type of quadrature implemented. In the rectangular quadrature we have implemented equidistant grid points with fixed spacing Δ_{\max} .

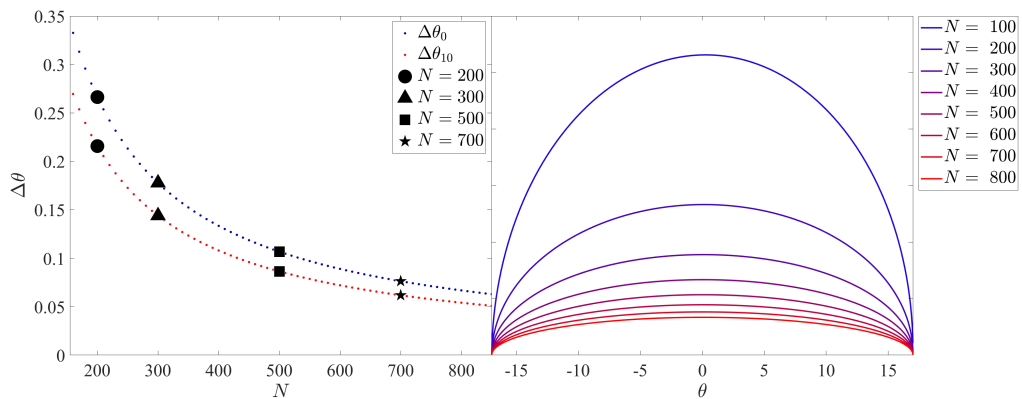


Figure 1: Right: The rapidity discretisation interval as a function of rapidity for different numbers of points in a fixed rapidity interval $\theta \in [-17, 17]$. The markers indicate the values of N that are considered in FIG. 5. Left: Comparison of the rapidity discretisation interval in the middle and towards the edges of the interval with non-trivial dynamics. $\Delta\theta_0$ and $\Delta\theta_{10}$ are defined to be the rapidity discretisation intervals for $\theta = 0$ and $\theta = 10$, respectively.

remains the largest for any value of N , the distribution quickly flattens out when the number of points is increased. Investigating the range of N values from 200 to 700, we achieve an order of magnitude increase in resolution for both $\theta = 0$ and 10. Significantly smaller is also the difference between these two quantities, which is consistent with the flattening of the curve in the right panel of FIG. 4. The numerical values of the size of the discretisation interval for a chosen numbers of points in the rapidity interval are included in Table III.

In order to obtain the averages of conserved charges and currents in the $SU(3)_2$ -HSG model, it is necessary to integrate over the rapidity variable, as defined in (4) of the paper. This integration procedure leads to the "accumulation" of any numerical errors present in the original function and to the formation of regular structures that could be easily mistaken for genuine physical phenomena. An example of this effect can be seen in the particle density associated to particle + computed with different rapidity discretisations. Four examples are presented in FIG. 5. As expected, the problem arises from the middle of the rapidity interval where resolution is lowest. By changing N we can identify a large enough value that guarantees a stable solution

N	$\Delta\theta_0$	$\Delta\theta_{10}$	$\Delta\theta_0 - \Delta\theta_{10}$
200	0.2664	0.2157	0.0506
300	0.1777	0.1439	0.0338
500	0.1067	0.0864	0.0203
700	0.0762	0.0617	0.0145

Table 3: Numerical values of the rapidity discretisation intervals $\Delta\theta$, for a given number of rapidity points N in the range of rapidities used in this investigation $\theta \in [-17, 17]$.

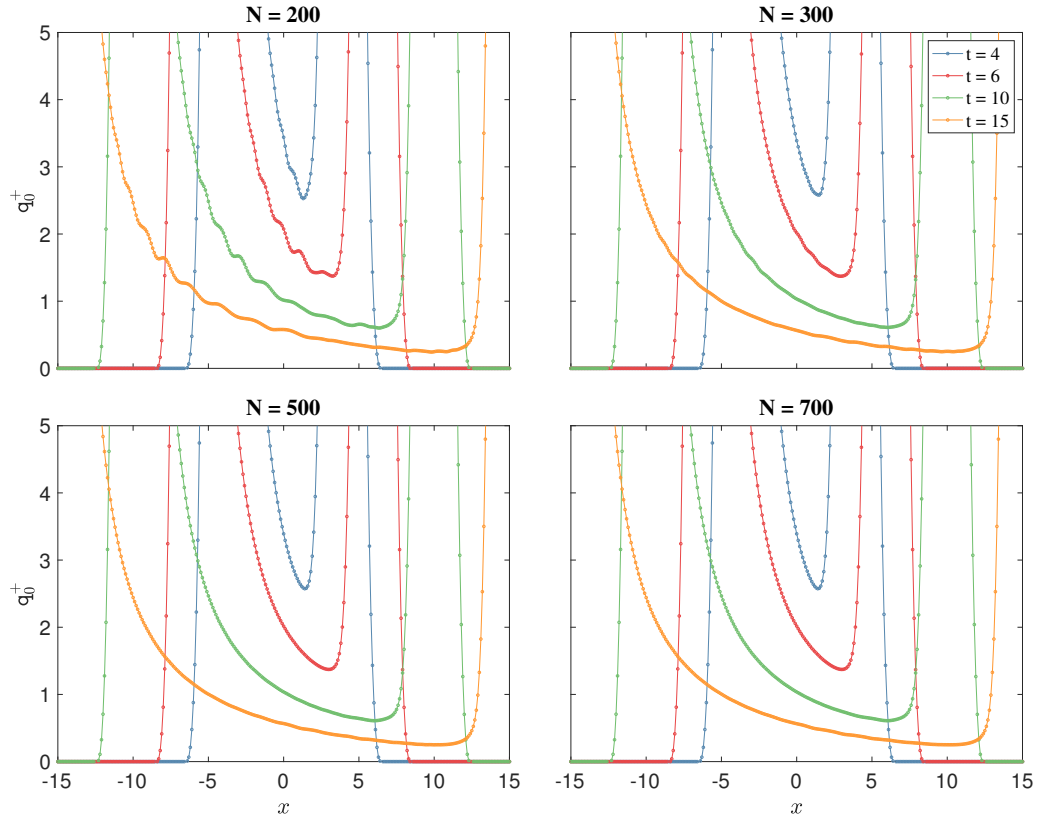


Figure 2: Spatial particle density of particle $+$ for different numbers of points in the fixed rapidity interval $\theta \in [-17, 17]$. The $N = 200$ panel shows regular oscillations. The oscillations persist for $N = 300$, disappear around $N = 500$ and are consistently absent for higher numbers of points, such as $N = 700$. Variations of space and time discretisation parameters have not produced any significant changes in the same functions.

for the spatial particle density. In our code we have chosen $N = 700$. The quantities not integrated over the rapidity integral did not exhibit any unusual behaviour even for the values of N as low as 200. Interestingly, this applies also to the spectral density, which produces then spatial particle density when integrated over rapidity. This further confirms that the emergence of the oscillations seen in the top left FIG. 5 is genuinely a numerical effect arising due to

integration.

References

- [1] F. S. Møller and J. Schmiedmayer, Introducing iFluid: a numerical framework for solving hydrodynamical equations in integrable models, *SciPost Phys.* **8**(3) (Mar 2020).
- [2] B. Doyon, H. Spohn, and T. Yoshimura, A geometric viewpoint on generalized hydrodynamics, *Nucl. Phys. B* **926**, 570–583 (Jan 2018).
- [3] O. A. Castro-Alvaredo, C. De Fazio, B. Doyon, and F. Ravanini, On the hydrodynamics of unstable excitations, *JHEP* **2020**(45) (2020).
- [4] O. A. Castro-Alvaredo, A. Fring, C. Korff, and J. L. Miramontes, Thermodynamic Bethe ansatz of the homogeneous sine-Gordon models, *Nucl. Phys. B* **575**, 535–560 (2000).
- [5] G. H. Golub and J. H. Welsch, Calculation of Gauss quadrature rules, *Math. Comp.* **23** (1969).
- [6] I. Bogaert, Iteration-free computation of Gauss–Legendre quadrature nodes and weights, *SIAM J. Sci. Comp.* **36** (2014).